Nanotechnology

Efficient Generation of Photocurrents by Using CdS/Carbon Nanotube Assemblies on Electrodes**

*Laila Sheeney-Haj-Ichia, Bernhard Basnar, and Itamar Willner**

The organization of functional semiconductor nanoparticles (NPs) on surfaces, and specifically electrodes, attracts substantial research efforts.[1] Semiconductor NP architectures on surfaces have been used to assemble photoelectrochemical cells,[2,3] to tailor light-emitting diodes,[4] to fabricate electrochromic devices,[5] and to organize sensor systems.[6,7] The photochemical excitation of semiconductor NPs to form an electron–hole pair is the primary event for the photocurrent generation. However, the transfer of conduction-band electrons to the electrode (or the supply of electrons from the electrode to the valence-band holes)—the processes that lead to the photocurrents—are hampered by the competing electron–hole recombination process, which degrades the

[*] L. Sheeney-Haj-Ichia, Dr. B. Basnar, Prof. I. Willner
Institute of Chemistry
The Hebrew University of Jerusalem
Jerusalem 91904 (Israel)
Fax: (+972) 2-652-7715
E-mail: willnea@vms.huji.ac.il

[**] This research is supported by the Israel Science Foundation (Project 101/00).

  DOI: 10.1002/ange.200461666

photogenerated species and prohibits the generation of the photocurrent. To enhance the photocurrent, the retardation of the recombination of the electron–hole species is essential. Different approaches to maximize charge separation in semiconductor NP architectures have been suggested. These include the use of molecular electron-relay semiconductor NP structures, in which the electron–hole is spatially separated by trapping the electrons in the relay units.[8,9] Conductive polymer films, which contact CdS nanoparticles with electrodes, act as efficient electron-transport matrices that retard the recombination reactions.[10] Hybrid composite semiconductor nanoclusters[11] or hybrid metal/semiconductor NP systems[12] were used for the enhanced generation of photocurrent. There the coupling of the two semiconductors CdS and SnO_2 resulted in improved photoelectrochemical properties of the hybrid material which were attributed to improved charge separation. The transfer of the CdS conduction-band electrons to the SnO_2 conduction band resulted in the separation of the electron–hole pair onto two different semiconductor particles. Similarly, the enhanced photocurrents[12] and photocatalytic properties[13] of metal/semiconductor composite nanostructures were attributed to the spatial separation of the electron–hole pair in the two nanoparticles.

Carbon nanotubes are an attractive material for application in electronic or sensor devices.[14] Carbon nanotubes (CNTs) are formed by the folding of graphite sheets, and the formation of conductive or semiconductive CNTs depends on the folding angle of the graphite sheets.[15] Conductive CNTs usually reveal high values of conductivity.[16] Different electronic applications of CNTs have been reported in recent years which include the organization of memory devices[17] or transistors.[18] Also, CNTs have been used as active sensing elements[19] and as building blocks of biosensors.[20] Numerous methods to functionalize the edges or ends of CNTs with chemical groups that enable the binding of the CNTs to other units or surfaces have been developed.[21,22] The organization of assemblies of CNT and semiconductor NP on electrodes might provide a new structure for improved photoelectrochemistry. To our knowledge, only one study has been reported on the assembly of a CNT/ZnO NP hybrid system,[23] but no function or photoelectrochemical properties of the system were addressed. Here we report the assembly of CdS NP/CNT hybrid systems on electrode surfaces. The system reveals efficient photoelectrochemical functions.

Fullerenes were previously employed as a carbon-based nanomaterial for photoelectrochemical applications.[24] The C_{60} nanostructure exhibits electron-acceptor properties. Its reversible redox activity was studied in detail,[25] and different photoelectrochemical studies have used C_{60} as an electron acceptor for mediated electron transport and the generation of photocurrents. For example, photoexcited polyphenylenevinylene polymers were used as electron donors for C_{60}, and the resulting composites resulted in the effective formation of photocurrents.[26] In stark contrast to C_{60}, CNTs do not display reversible electrochemistry and do not exhibit electron-acceptor features. The documented high conductivity of CNTs (1.0×10^{6}–$3.0\times10^{6}\,S\,m^{-1}$)[16] renders them conductive nanowires rather than charge traps. Thus, the enhanced photocurrents in the present system originate from improved electron transport through the conductive wires in contrast to the mediated electron transfer in the C_{60} systems.

Scheme 1 depicts the method to assemble the CdS/CNT monolayer on a Au electrode. The CNTs were purified and

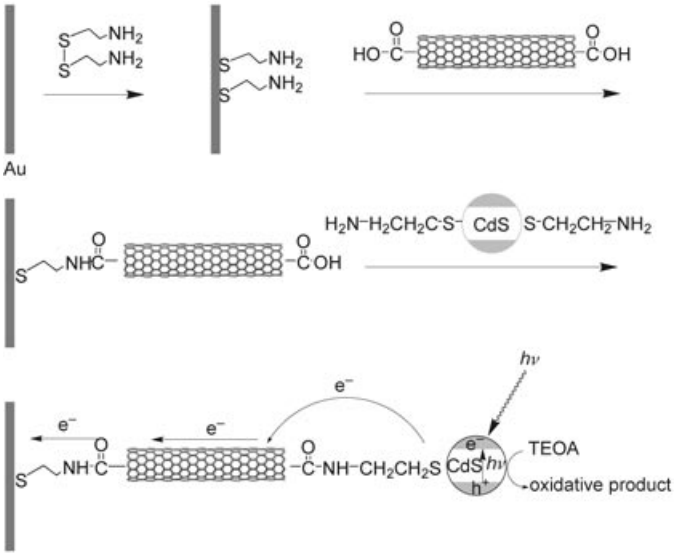

Scheme 1. The assembly of the CdS NP/CNT system on a Au electrode, and the photoinduced charge transport in the system. TEOA = triethanolamine, h^+ = hole.

"cut" by using a mixture of concentrated sulfuric and nitric acids (3:1, 98 % and 70 %, respectively) to yield CNTs with an average length of $\approx$10–100 nm as determined by TEM experiments. This procedure introduces carboxylic acid functionalities at the ends of the CNTs as well as some carboxylic acid units at the CNT sidewalls. The Au electrode was functionalized with a primary monolayer of cysteamine to which the CNTs were then coupled. The CdS NPs (5 nm, protected a capping monolayer of cysteamine and 2-thioethanesulfonic acid) were then coupled to the ends of the CNTs.

Microgravimetric quartz crystal microbalance (QCM) analyses allowed the surface coverage of the components to be characterized. The modification of the surface with the CNTs is controlled by the duration of the coupling process. Figure 1 shows the frequency changes (Δf) that occurred upon modification of the cysteamine monolayer-functionalized Au surface with the CNTs that were cut for a period of 4 h in acid solution. After $\approx$4 h of coupling, the frequency change reaches a constant value that translates to a weight coverage of $\approx3.14\times10^{-6}\,g\,cm^{-2}$ ($\Delta f=-575$ Hz). The CNT-functionalized surface was then modified with the CdS NPs. The absorbance spectrum of the CdS NPs revealed a shoulder at $\approx$400 nm which is consistent with the size of the NPs. The CdS NPs were then coupled to the CNTs associated with the electrode in the presence of 1-ethyl-3-(3-dimethyaminopropyl)carbodiimide (EDC). The microgravimetric analysis of the coupling of the CdS NPs to the CNTs assembled on a Au/quartz crystal (2 h of coupling) indicated a frequency change of -270 Hz that corresponds to a surface coverage of $\approx4.7\times$

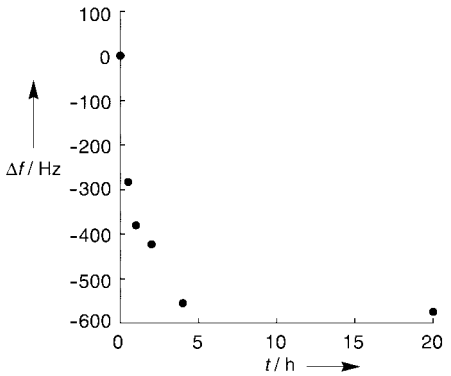

Figure 1. Time-dependent frequency changes (Δf) of a cysteamine-functionalized Au/quartz crystal upon the coupling of CNTs that had undergone oxidative digestion for 4 h. The coupling was performed with dicyclohexylcarbodiimide (0.01 M) in DMF in the presence of the CNT (5 mg mL^{-1}). Frequencies were recorded in air.

10^{12} particles cm^{-2}. Further evidence for the coupling of the CdS NPs to the surface was obtained from X-ray photoelectron spectroscopic (XPS) measurements. After the modification of the CNT interface with the CdS NPs for 2 h, the electrons characteristic of Cd(3d), C(1s), and Au(4f) at 404, 283.8, and 82.65 eV, respectively, were observed in a ratio of 4.1:48.9:21.0%. After 4 h of modification, the coverage of the CdS NPs increased as seen by the ratio of the intensities 4.3:50.1:15.9% for the Cd(3d), C(1s), and Au(4f) electrons, respectively.

The assembly of the CdS NPs and CNTs on the surface was also characterized by AFM. Figure 2a shows the image of the CNTs that were covalently linked to a Au surface during a modification time of 10 minutes (CNTs generated by acidic digestion for 4 h were used in this experiment). Vertically aligned (standing) CNTs are observed with a maximum height of $\approx$20 nm. By allowing longer durations for the modification step, high-density coverage of the surface by the CNTs was observed. Figure 2b shows the AFM image of the surface after the covalent attachment of the CdS NPs. Higher objects ($\approx$25 nm) are observed which suggests that the semiconductor NPs are linked to the ends of the CNTs (it is impossible to exclude the binding of the CdS NPs to the sidewalls of the CNTs). Figure 2c shows the AFM image of a surface modified with CdS NPs which was obtained after coupling to the CNT-modified Au surface during 4 h. From the surface area of the electrode and the size of the CdS NPs, a random and densely packed monolayer of NPs was observed with a surface coverage of $\approx 4.5 \times 10^{12}$ particles cm^{-2}. The microgravimetric analyses of the surface revealed a surface coverage of $\approx 4.7 \times 10^{12}$ particles cm^{-2}. This value, taken together with the AFM image, suggests that a densely packed monolayer of the semiconductor NPs is associated with the electrode. The AFM images of the CNTs that were linked to the surface during short modification periods (Figure 2a and b) show heights of 10 to 30 nm, whereas the TEM image reveals a substantially higher dispersity of 10 to 100 nm. This may originate from the relatively low concentration of longer CNTs in the mixture and the lower reactivity of the longer CNTs in the coupling process. In fact, similar

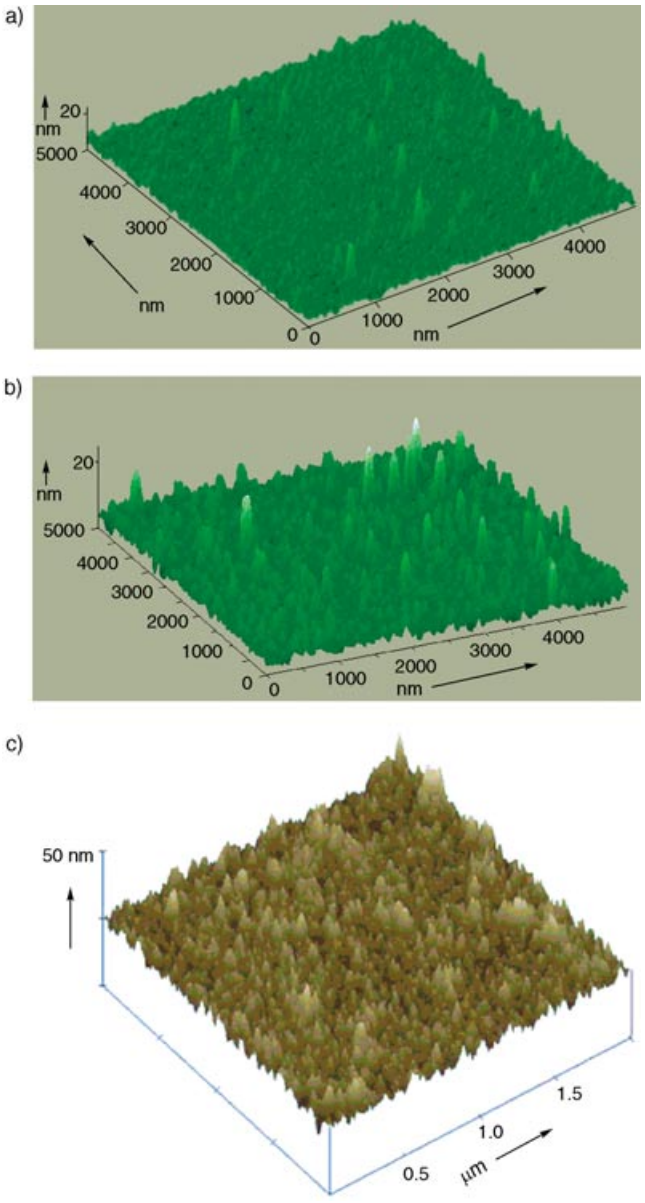

Figure 2. AFM images of the cysteamine-functionalized Au surface upon a) the coupling of CNTs (reaction time: 10 min; oxidative digestion: 4 h), b) after the subsequent coupling of the modified CdS NPs (reaction time:2 h), and c) after the coupling of the CNTs (oxidative digestion: 4 h) to the surface (reaction time: 4 h) and the subsequent binding of the CdS NPs (reaction time: 2 h).

AFM results were previously reported for CNT-modified surfaces that employed CNT prepared by an analogous procedure to the present study.[21]

The photoelectrochemical properties of the CdS NP/CNT-functionalized electrodes, which were generated from CNTs that were digested in the acidic solution for 4 h, were examined. The photocurrent generated by the functionalized electrode in the presence of triethanolamine as a sacrificial electron donor was examined in an electrolytic aqueous phosphate buffer solution (0.1 M, pH 10). The resulting photocurrent action spectrum is depicted in Figure 3, curve (a). The photocurrent spectrum follows the profile of the absorption

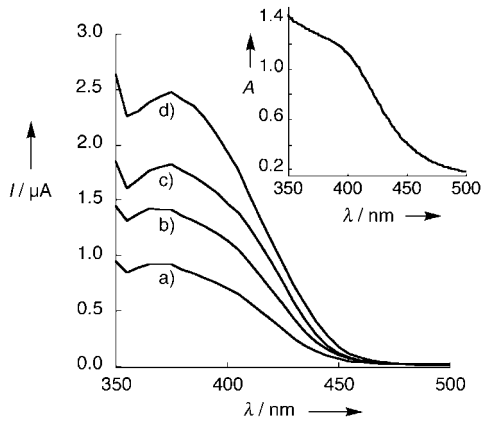

Figure 3. Photocurrent action spectra observed with Au electrodes modified with CdS NP/CNT systems, in which the CNTs were allowed to undergo oxidative digestion during a) 4 h, b) 6 h, c) 8 h, or d) 10 h. In all of the experiments, the resulting CNT interfaces were treated with the CdS NPs during 2 h. Photocurrent spectra were recorded in phosphate buffer solution (0.1 M, pH 10) that contained triethanolamine (0.02 M). Inset: Absorbance spectrum of the CdS nanoparticles (5 nm) capped with cysteamine/2-thioethanesulfonic acid (1:10).

spectrum of the CdS NPs which indicates that it originates from the excitation of the semiconductor NPs. No photocurrent is generated in the absence of triethanolamine. In a control experiment, no photocurrent was observed upon irradiation of a CNT-functionalized electrode that lacked the CdS NPs in the presence of triethanolamine. This result indicates that the photocurrent originates from the CdS NPs and that the CNTs are not photoactive in the process. The generated photocurrent is, however, impressively high, $I(\lambda_{390}) = 0.83\ \mu A$, for the CNT/CdS NP monolayer. From the intensity of the light absorbed by the sample, we estimate that the quantum efficiency for the photon-to-electron conversion is 25%.

In a further control experiment, a monolayer of CdS NPs was assembled on a Au electrode by the covalent coupling of the NPs to an electrode functionalized with a monolayer of cysteic acid. The microgravimetric characterization of the assembly of the monolayer on a Au/quartz crystal indicated a surface coverage of 5.1×10^{12} particles cm^{-2}. Although the surface coverage of the NPs in the monolayer assembly is very similar to that observed in the CdS NPs/CNT system, the photocurrent generated by the system that lacks the CNT connectors is substantially lower, $I(\lambda_{390}) = 0.05\ \mu A$, and the photon-to-electron quantum efficiency is $\approx 1.5\%$. Thus, we conclude that the CNTs which bridge the CdS NPs to the electrode play a major role in the enhanced generation of photocurrents.

We further examined the effect of the lengths of the CNTs on the resulting photocurrent. It is established that the longer time intervals of acidic digestion of the CNTs yields shorter tubes. Accordingly, we digested the CNTs for different lengths of time and used the resulting CNTs to assemble the bridged CdS NP-functionalized electrodes. Unfortunately, we were unable to determine the lengths of the CNTs obtained upon the acidic digestion process owing to a broad dispersity. Thus, we assume that prolongation of the digestion time leads to a decrease in the length of the CNTs (without actual quantification of the length of the bridging units). Figure 3 shows the photocurrents generated by the CdS NP/CNT-functionalized electrodes, which consist of CNTs that were acid-digested for different lengths of time, as bridging units. The photocurrent action spectra follow the profile of the absorbance spectrum of the CdS NPs (see Figure 3, Inset) which implies that the photocurrent originates from the excitation of the semiconductor NPs. The photocurrents obtained reveal that the photocurrent is enhanced as the digestion time of the CNTs is increased (shorter linking CNTs). Table 1 summarizes the surface coverage, the photocurrent intensities at $\lambda = 390$ nm, and the photon-to-electron quantum efficiencies of the CdS NPs in the systems with the different CNTs. The quantum efficiencies increase as the digestion time increases (shorter CNTs), and for CNTs digested for 4, 6, 8, and 10 h, the quantum yields correspond to 25, 39, 51, and 70%. From the data in Table 1 we see that the surface coverages of the CdS NPs in the different systems are comparable.

Table 1: Microgravimetric quartz-crystal-microbalance analyses of the CdS/CNT systems assembled on Au/quartz crystals and the respective surface coverage values.

System[a]	Δf [Hz] SWCNT	Δm [$g\,cm^{-2}$]	Δf [Hz] CdS NP	Particles [cm^2]
a	−575	3.14×10^{-6}	−270	4.66×10^{12}
b	−520	2.83×10^{-6}	−310	5.34×10^{12}
c	−450	2.45×10^{-6}	−238	4.12×10^{12}
d	−320	1.74×10^{-6}	−287	4.96×10^{12}
CdS monolayer[b]			−294	5.07×10^{12}

[a] The different systems comprise CNTs that were subjected to oxidative digestions during a) 4 h, b) 6 h, c) 8 h, or d) 10 h. [b] The surface loading of a CdS NP system directly coupled to the electrode is provided for comparison.

The results clearly demonstrate the very efficient generation of photocurrents in the CNT-bridged CdS NP assemblies. Although we have no firm explanation for the enhanced photocurrents, we speculate and suggest a possible origin for these observations on the basis of the known properties of CNTs. The photocurrent originates from the photoexcitation of the semiconductor NPs which yields an electron–hole pair. The injection of the conduction-band electrons into the electrode yields the photocurrent, whereas the electron donor (in solution) provides the electrons to the valence-band holes to thus complete the photocurrent generation cycle (see Scheme 1). The electron–hole recombination is a competing process to the electron-injection mechanism, and thus the photocurrent efficiency is low. The CNT connectors which bridge the CdS NPs to the electrode may then facilitate the photocurrent generation by trapping the conduction-band electrons, a process that results in charge separation and retardation of the recombination process. That is, the conductive CNT wires provide efficient paths for the transport of the conduction-band electrons to the electrode. This

explanation, based on the conductance of the CNT connector is, however, contradicted by the observation of a dependence on the length of the CNT. Whereas charge-transport rates in ideal CNTs should be almost length-independent, the CNTs employed in the present study are far-from-ideal wrapped graphite sheets. The oxidative acidic digestion of the CNTs not only shortens the CNTs, but it introduces defects into the sidewalls, which consist of phenolic, ketone, or carboxylic acid functionalities. These units disrupt the conjugation within the graphite sheets and act as local defect sites for charge transport.

The effect of defects in CNTs on the charge-transport properties has been considered theoretically by using a "back-scattering" model.[27] According to this model, as the electron reaches a defect site, it is back-scattered to find an alternative conjugated path to be transported along the CNT. As the number of defects in the CNT increases with its length, charge transport along the CNT will be dominated by its length. That is, the charge injection of the conduction-band electrons to the CNTs, leads to charge separation by entrapment of the electrons in the CNT wire. The chemically generated local defects in the CNTs affect, however, the efficiency of the charge separation. As the CNTs are longer, more defects exist in the connecting wires and thus the back-scattering process retards the conductance of the trapped electrons to the electrode. The trapped electrons in the CNTs can then recombine with the valence-band holes to result in lower quantum yields for the photon-to-electron conversion process as the CNTs become longer.

An alternative mechanism for the observed enhanced photocurrent in the system is based on the semiconductive properties of the CNTs. The band-gap structure of CNTs has been studied,[28] and interparticle–CNT electron transfer could lead to charge separation and enhanced photocurrents. The low population of semiconductive CNTs in the carbon nanotube mixture, and particularly the enhanced photocurrents observed with shorter CNTs, probably exclude any function of the semiconductive CNTs in the enhanced generation of photocurrents. For shorter CNTs, larger band gaps are formed which would perturb the interparticle–CNT electron-transfer process. Thus, if semiconductive CNTs participate in the generation of photocurrents, one would anticipate to observe lower yields of photocurrents for shorter CNTs, in contrast to the experimental observations.

In conclusion, the present study has demonstrated unprecedented high quantum yields for the generation of photocurrents by using semiconductor nanoparticles/carbon nanotubes as a hybrid system. The results suggest that the length of the CNTs plays a major role in the formation of photocurrents and probably the defects in the CNT affect the extent of charge separation that follows the photoexcitation of the CdS NPs. More experiments which employ CNTs of low length dispersity are underway to further characterize the system.

Experimental Section

Single-walled CNTs (SWCNTs; Carbolex, Sigma) were purified by heating the as-received nanotubes in nitric acid (3 M) at reflux for 48 h. The resulting CNTs were isolated by centrifugation and rinsed with NaOH solution (1 mM) until pH 7.0. The purified long SWCNTs were then chemically shortened by oxidation in a mixture (3:1) of concentrated sulfuric acid (98%) and nitric acid (70%): the samples were sonicated in an ice/water bath during 4, 6, 8, or 10 h. The solutions containing the SWCNTs were centrifuged, then the samples were washed with NaOH solution (1 mM) until pH 7.0, and the CNTs were then dissolved in DMF (*N*,*N*-dimethylformamide). This procedure yielded shortened SWCNTs with terminal carboxylate groups.

Cysteamine-protected CdS nanoparticles were prepared according to a reported procedure.[12b] The surface of a Au electrode was modified with a monolayer of a mixture of 2-thioethanol and cystamine (3:1 ratio), and the shortened SWCNTs were covalently linked to the amino groups of the cysteamine monolayer-functionalized Au surface in the presence of dicyclohexylcarbodiimide (DCC; 1×10^{-2} M) in DMF (2-thioethanol was incorporated in the mixed monolayer to prevent nonspecific adsorption of the SWCNTs onto the electrode surface and also to prevent the coupling of the SWCNTs through their sidewalls to the surface). The modified electrodes were treated with a solution of cysteamine-stabilized CdS nanoparticles (1 mg mL^{-1}, 2 mL) in HEPES buffer, which included 1-ethyl-3-(3-dimethyaminopropyl)carbodiimide (EDC), for 2 h. The assembly of the CdS monolayer on the Au surface was prepared according to the published procedure.[12b]

Microgravimetric QCM measurements were performed with a QCM analyzer (Fluke) by using Au/quartz crystals (AT-cut, 10 MHz). Photoelectrochemical experiments were performed with a home-built photoelectrochemical system that includes a 300W Xe lamp (Oriel, model 5258), a monochromator (Oriel, model 74000, 2-nm resolution), and a chopper (Oriel, model 76994). XPS analyses were performed with a Kratos AXIS-HS spectrometer equipped with a monochromatic $Al_{K\alpha}$ source. Usually scans were run at 45 or 75 W. All data acquisitions were performed in a hybrid mode by using electrostatic and magnetic lenses and detection pass energies of 40–80 eV. AFM images were recorded in the tapping mode in air with a Smena B instrument (NT-MDT, Russia), with a 30-μm scanner, NCS-16 cantilevers (resonance frequency 180 KHz), a scan rate of 1.5–2.5 Hz, and a cantilever oscillation amplitude of the order of 20–40 nm.

Received: August 16, 2004
Revised: September 1, 2004

Keywords: electrochemistry · electron transport · monolayers · nanotubes · semiconductors

[1] a) A. N. Shipway, E. Katz, I. Willner, *ChemPhysChem* **2000**, *1*, 18–52; b) M.-C. Daniel, D. Astruc, *Chem. Rev.* **2004**, *104*, 293–346.

[2] a) S. G. Hickey, D. J. Riley, E. J. Tull, *J. Phys. Chem. B* **2000**, *104*, 7623–7626; b) M. Miyake, T. Torimoto, T. Sakata, H. Mori, H. Yoneyama, *Langmuir* **1999**, *15*, 1503–1507.

[3] H. Jensen, D. J. Fermin, J. E. Moser, H. H. Girault, *J. Phys. Chem. B* **2002**, *106*, 10908–10914.

[4] a) B. O. Dabbousi, M. G. Bawendi, O. Onitsuka, M. F. Rubner, *Appl. Phys. Lett.* **1995**, *66*, 1316–1318; b) H. Mattoussi, L. H. Radzilowski, B. O. Dabbousi, E. L. Thomas, M. G. Bawendi, M. F. Rubner, *J. Appl. Phys.* **1998**, *83*, 7965–7974; c) N. Tessler, V. Medvedev, M. Kazes, S. H. Kan, U. Banin, *Science* **2002**, *295*, 1506–1508.

[5] C. Bechinger, S. Ferrer, A. Zaban, J. Sprague, B. A. Gregg, *Nature* **1996**, *383*, 608–610.

[6] F. Patolsky, R. Gill, Y. Weizmann, T. Mokari, U. Banin, I. Willner, *J. Am. Chem. Soc.* **2003**, *125*, 13918–13919.

[7] a) V. Pardo-Yissar, E. Katz, J. Wasserman, I. Willner, *J. Am. Chem. Soc.* **2003**, *125*, 622–623; b) I. Willner, F. Patolsky, J.

Wasserman, *Angew. Chem.* **2001**, *113*, 1913 – 1916; *Angew. Chem. Int. Ed.* **2001**, *40*, 1861 – 1864.
[8] L. Sheeney-Haj-Ichia, J. Wasserman, I. Willner, *Adv. Mater.* **2002**, *14*, 1323 – 1326.
[9] L. Sheeney-Haj-Ichia, I. Willner, *J. Phys. Chem. B* **2002**, *106*, 13094 – 13097.
[10] E. Granot, F. Patolsky, I. Willner, *J. Phys. Chem. B* **2004**, *108*, 5875 – 5881.
[11] a) A. Zaban, S. G. Chen, S. Chappel, B. A. Gregg, *Chem. Commun.* **2000**, 2231 – 2232; b) P. A. Sant, P. V. Kamat, *Phys. Chem. Chem. Phys.* **2002**, *4*, 198 – 203; c) C. Nasr, S. Hotchandani, W. Y. Kim, R. H. Schmehl, P. V. Kamat, *J. Phys. Chem. B* **1997**, *101*, 7480 – 7487.
[12] a) V. Subramanian, E. Wolf, P. V. Kamat, *J. Phys. Chem. B* **2001**, *105*, 11439 – 11446; b) L. Sheeney-Haj-Ichia, S. Pogorelova, Y. Gofer, I. Willner, *Adv. Funct. Mater.* **2004**, *14*, 416 – 424.
[13] V. Subramanian, E. E. Wolf, P. V. Kamat, *J. Am. Chem. Soc.* **2004**, *126*, 4943 – 4950.
[14] a) E. Katz, I. Willner, *ChemPhysChem* **2004**, *5*, 1084 – 1104; b) J. J. Davis, K. S. Coleman, B. R. Azamian, C. B. Bagshaw, M. L. H. Green, *Chem. Eur. J.* **2003**, *9*, 3732 – 3739.
[15] a) A. Hirsch, *Angew. Chem.* **2002**, *114*, 1933 – 1939; *Angew. Chem. Int. Ed.* **2002**, *41*, 1853 – 1859; b) S. Iijima, *Physica B* **2002**, *323*, 1 – 5.
[16] a) J. E. Fischer, H. Dai, A. Thess, R. Lee, N. M. Hanjani, D. L. Dehaas, R. E. Smalley, *Phys. Rev. B* **1997**, *55*, R4921 – R4924; b) D. H. Cobden, M. Bockrath, P. L. McEuen, A. G. Rinzler, R. E. Smalley, *Phys. Rev. Lett.* **1998**, *81*, 681 – 684.
[17] a) T. Rueckes, K. Kim, E. Joselevich, G. Y. Tseng, C. L. Cheung, C. M. Lieber, *Science* **2000**, *289*, 94 – 97; b) N. Mason, M. J. Biercuk, C. M. Marcus, *Science* **2004**, *303*, 655 – 658.
[18] a) S. J. Tans, A. R. M. Verschueren, C. Dekker, *Nature* **1998**, *393*, 49 – 52; b) R. Martel, T. Schmidt, H. R. Shea, T. Hertel, P. Avouris, *Appl. Phys. Lett.* **1998**, *73*, 2447 – 2449.
[19] a) J. Wang, M. Musameh, *Anal. Chem.* **2003**, *75*, 2075 – 2079; b) J. Wang, S. B. Hocevar, B. Ogorevc, *Electrochem. Commun.* **2004**, *6*, 176 – 179; c) K. Bradley, M. Briman, A. Star, G. Grüner, *Nano Lett.* **2004**, *4*, 253 – 256; d) A. Star, J.-C. P. Gabriel, K. Bradley, G. Grüner, *Nano Lett.* **2003**, *3*, 459 – 463.
[20] a) F. Patolsky, Y. Weizmann, I. Willner, *Angew. Chem.* **2004**, *116*, 2165 – 2169; *Angew. Chem. Int. Ed.* **2004**, *43*, 2113 – 2117; b) K. Besteman, J.-O. Lee, F. G. M. Wiertz, H. A. Heering, C. Dekker, *Nano Lett.* **2003**, *3*, 727 – 730.
[21] a) P. Diao, Z. Liu, B. Wu, X. L. Nan, J. Zhang, Z. Wei, *ChemPhysChem* **2002**, *3*, 898 – 901; b) Z. Liu, Z. Shen, T. Zhu, S. Hou, L. Ying, Z. Shi, Z. Gu, *Langmuir*, **2000**, *16*, 3569 – 3573; c) J. J. Gooding, R. Wibowo, J. Liu, W. Yang, D. Losic, S. Orbons, F. J. Mearns, J. G. Shapter, D. B. Hibbert, *J. Am. Chem. Soc.* **2003**, *125*, 9006 – 9007.
[22] a) K. Jiang, L. S. Schadler, R. W. Siegel, X. Zhang, H. Zhang, M. Terrones, *J. Mater. Chem.* **2004**, *14*, 37 – 39; b) M. J. Moghaddam, S. Taylor, M. Gao, S. Huang, L. M. Dia, M. J. H. McCall, *Nano Lett.* **2004**, *4*, 89 – 93; c) M. Hazani, R. Naaman, F. Hennrich, M. M. Kappes, *Nano Lett.* **2003**, *3*, 153 – 155; d) H. Peng, L. B. Alemany, J. L. Margrave, V. N. Khabasheku, *J. Am. Chem. Soc.* **2003**, *125*, 15174 – 18182.
[23] a) J. Sun, L. Gao, M. Iwasa, *Chem. Commun.* **2004**, 832 – 833; b) B. R. Azamian, K. S. Coleman, J. J. Davis, N. Hanson, M. L. H. Green, *Chem. Commun.* **2002**, 366 – 367.
[24] a) S. Licht, O. Khasclev, P. A. Ramakrishnan, D. Faiman, E. A. Katz, A. Shames, S. Goren, *Solar Energ. Mater. Solar Cells* **1998**, *51*, 9 – 19; b) P. V. Kamat, M. Gavaert, K. Vinodgopal, *J. Phys. Chem. B* **1997**, *101*, 4422 – 4427.
[25] R. E. Hauflter, J. Conceicao, L. P. F. Chibamte, Y. Chai, N. E. Byrne, S. Flanagan, M. M. Haley, S. C. O′Brien, C. Pan, Z. Xiao, W. E. Billups, M. A. Ciufolini, R. H. Hauge, J. L. Margrave, L. J. Wilson, R. F. Curl, R. E. Smalley, *J. Phys. Chem.* **1999**, *103*, 8634 – 8636.
[26] a) C. H. Lee, G. Yu, D. Moses, K. Pakbaz, C. Zhang, N. S. Sariciftci, A. J. Heeger, F. Wudl, *Phys. Rev. B* **1993**, *48*, 15425 – 15433; b) L. Smilowitz, N. S. Sariciftci, R. Wu, C. Gettinger, A. J. Heeger, F. Wudl, *Phys. Rev. B* **1993**, *47*, 13835 – 13842.
[27] V. Mujica, A. Nitzan, Y. Mao, W. Davis, M. Kemp, A. Roitberg, M. A. Ratner, *Physics* **1997**, *107*, 403 – 429.
[28] a) T. Nakanishi, A. Bachtold, C. Dekker, *Phys. Rev. B* **2002**, *66*, 073307; b) L. C. Venema, J. W. Janssen, M. R. Buitelaar, J. W. G. Wildöer, S. G. Lemay, L. P. Kouwenhoven, C. Dekker, *Phys. Rev. B* **2000**, *62*, 5238 – 5244.

